

# Nanoscale Confinement of Dip-Pen Nanolithography Written Phospholipid Structures on CuZr Nanoglasses

Srivatsan K. Vasantham, Evgeniy Boltynjuk, Sree Harsha Nandam, Eider Berganza Eguiarte, Harald Fuchs,\* Horst Hahn,\* and Michael Hirtz\*

Nanoglasses have attracted considerable interest among material scientists due to their novel and surprising properties. However, there is still a significant gap in understanding how nanoglasses interact with biomaterials and their effects on living cells. Previous cell studies have reported indications of possible proliferation effects, but a comprehensive understanding of differentiating nanoglass influences from distinct material or topography effects is yet to be established. In this study, the interaction between nanoglass surfaces and phospholipids, which are fundamental components of cell membranes, is investigated. The findings reveal a unique stabilizing effect exhibited by nanoglasses on structures created using lipid dip-pen nanolithography, preventing their spreading over the surface (“confinement”). This discovery suggests that nanoglasses can potentially influence the structure of cell membranes, providing a conceivable mechanism for how nanoglasses may impact cell behavior.

structures, separated by interfacial defects. These glasses have been termed nanoglasses because of their internal structuring on the nanometer scale.<sup>[1]</sup> In their nanostructure, such glasses resemble the structure of nanocrystalline materials with crystalline grains and grain boundaries, however, in the case of nanoglasses, the two components, cores (similar to the crystalline grains in nanocrystalline materials) and interfaces (similar to the grain boundaries in nanocrystalline materials) are amorphous. These two components exhibit distinctly different atomic short- and medium-range order and density. Nanoglasses are produced mainly using bottom-up methods, such as inert gas condensation (IGC),<sup>[2,3]</sup> and magnetron sputtering (MS).<sup>[4,5]</sup> In IGC, amorphous


nanoparticles are compacted into bulk pellets at high pressures to form the amorphous interfaces between the particles (clusters). For this study, the nanoglasses were prepared in the form of thin films with a columnar nanostructure using MS. (Figure 1a). So far, nanoglasses have been synthesized from a wide range of binary alloys: Si–M (M = Pd, Fe, Au, La), Ti–Pd, Au–La, Fe–Sc, e.g., Cu–Zr,<sup>[6]</sup> Ni–Ti<sup>[7]</sup>; as well as multi-component systems, Au–Ag–Pd–Cu–Si–Al,<sup>[4]</sup> Ti–Zr–Be–Fe–Cu.<sup>[8]</sup>

## 1. Introduction

Metallic glasses lack crystalline long-range order and therefore cannot have crystal defects, such as grain boundaries. In that sense, homogenous metallic glasses are more uniform in chemical composition and microstructure than crystalline materials. An alternative to a homogenous metallic glass has been developed, which is constituted of nanometer-sized grain-like

S. K. Vasantham, E. Boltynjuk, S. H. Nandam, E. Berganza Eguiarte, H. Hahn, M. Hirtz  
 Institute of Nanotechnology (INT)  
 Karlsruhe Institute of Technology (KIT)  
 Hermann-von-Helmholtz-Platz 1, 76344 Eggenstein-Leopoldshafen, Germany  
 E-mail: horst.hahn@kit.edu; michael.hirtz@kit.edu

S. K. Vasantham, M. Hirtz  
 Karlsruhe Nano Micro Facility (KNMFi)  
 Karlsruhe Institute of Technology (KIT)  
 Hermann-von-Helmholtz-Platz 1, 76344 Eggenstein-Leopoldshafen, Germany

 The ORCID identification number(s) for the author(s) of this article can be found under <https://doi.org/10.1002/admi.202300721>

© 2023 The Authors. Advanced Materials Interfaces published by Wiley-VCH GmbH. This is an open access article under the terms of the Creative Commons Attribution License, which permits use, distribution and reproduction in any medium, provided the original work is properly cited.

DOI: 10.1002/admi.202300721

S. H. Nandam  
 Department of Metallurgical Engineering  
 Indian Institute of Technology (BHU)  
 Varanasi 221005, India  
 H. Fuchs  
 Physical Institute  
 University of Münster  
 Wilhelm-Klemm-Straße 10, 48149 Münster, Germany  
 E-mail: fuchsh@uni-muenster.de

H. Fuchs  
 Center for Nanotechnology (CeNTech)  
 University of Münster  
 Heisenbergstraße 11, 48149 Münster, Germany  
 H. Hahn  
 Chemical, Biological and Materials Engineering  
 The University of Oklahoma  
 201 Stephenson Pkwy., Norman, OK 73019, USA

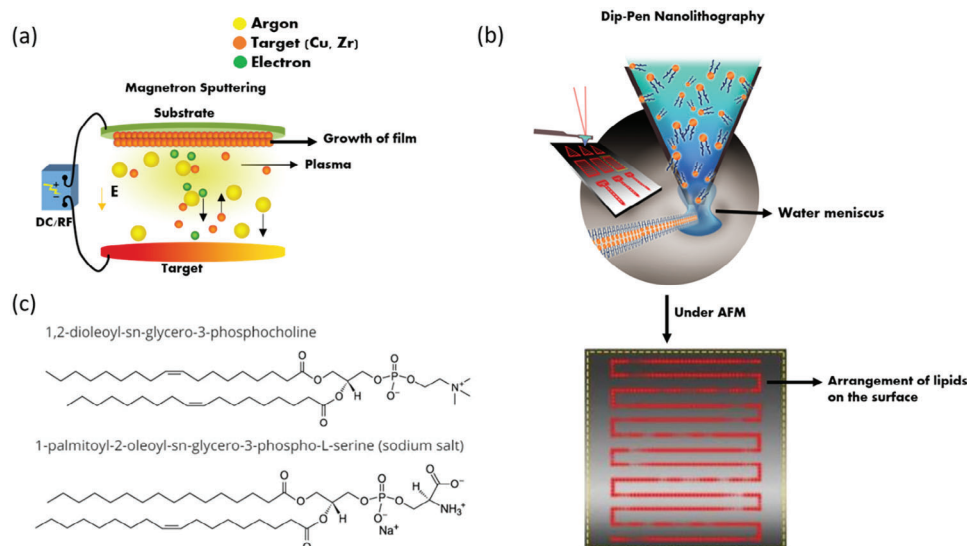


**Figure 1.** Schematic illustration of the a) magnetron sputtering and b) Lipid dip-pen nanolithography processes. c) Chemical structure of the written phospholipids (DOPC and POPS).

In particular, Zr–Pd<sup>[9]</sup> and Ti<sub>34</sub>Zr<sub>14</sub>Cu<sub>22</sub>Pd<sub>30</sub><sup>[10]</sup> nanoglasses have been demonstrated to possess properties suitable for biomedical applications. Both nanoglasses feature a cauliflower-like hierarchical structure, where small building blocks are divided by interfacial regions and are organized in agglomerates, which in turn form large clusters separated by thicker interfaces. These structures have multiple defining parameters such as the size of the small building blocks, the volume fraction of interfacial regions, the size of agglomerates, and the volume fraction of thicker interfaces.

For the purpose of studying lipid-surface interaction, we aimed to reduce these variables. CuZr nanoglass thin films can be created with varying sizes of evenly distributed columns by adjusting synthesis parameters. Our efforts led to the fabrication of CuZr nanoglass structures with column sizes of 16 and 60 nm. This advancement enables a deeper study into how the columnar structure influences lipid behavior by comparing homogeneous to columnar films. Additionally, we can assess how column size, specifically films with 16 and 60 nm columns, affects lipid confinement (stabilizing lipid features against spreading out on the surface) and arrangement.

Generally, nanostructured surfaces are known to have a strong influence on cell adhesion and can modulate the behavior, proliferation, and fate of cells.<sup>[4,11–13]</sup> Also, nanotopographical structures have been shown to play a vital role in other bio-applications.<sup>[14,15]</sup> In this regard, nanoglasses offer a unique opportunity for combining material and topographical cues, and it was previously reported that a Ti-based nanoglass shows a higher proliferation in osteoblasts compared to a conventional (homogeneous) metal glass of identical chemical composition.<sup>[10]</sup> The identification of possible reasons for this striking difference between the different amorphous structures, and the exploration of the effects of topography and material, are considered to be challenging problems. There are various pathways and mechanisms for the interaction and subsequent behavioral modulation of cells in contact with nanotopographies or structures, including con-

tact guidance, membrane curvature, modulation of various different membrane proteins, like channel proteins or integrins, or topography-induced changes to the cytoskeleton.<sup>[11,16–18]</sup> Generally, cells interact with the surface through their outer membrane, consisting of a complex of phospholipids (as structural building blocks) and a plethora of proteins with various functions in adhesion, material exchange between the inside and outside of the cell and signaling. As the state of the structural membrane can modulate the function of proteins<sup>[19]</sup> and plays a role in cell sensing of their environment,<sup>[20]</sup> the interaction of phospholipids with nanoglass surfaces and the resulting change in the lipid membrane might be a crucial piece of information as a first step to understand their interactions with cells.

Consequently, in this paper, we explore the interaction of Cu<sub>60</sub>Zr<sub>40</sub> nanoglasses produced by MS with biomimetic lipid membranes written by dip-pen nanolithography<sup>[21,22]</sup> with phospholipids (L-DPN).<sup>[23]</sup> Dip-pen nanolithography for patterning lipids has been used on a wide variety of substrates such as silicon, glass, polymer, graphene, polystyrene, and titanium.<sup>[23–25]</sup> L-DPN utilizes an atomic force microscopy (AFM) tip, dipped into a lipid mixture as ink (with 1,2-dioleoyl-sn-glycero-3-phosphocholine (DOPC) as a main carrier), to deposit biomimetic lipid membranes onto surfaces (Figure 1b). Previously, L-DPN has been used for biomedical applications such as drug delivery, cell culture, biomarker detection and cancer cell detection, and protein screening.<sup>[26–29]</sup> Also, the overall behavior of these lipid membranes on different substrates is influenced by wetting properties, roughness, and morphology, thus they can act as a probe for surfaces.<sup>[24,30–32]</sup>

## 2. Results and Discussion

### 2.1. Synthesis and Characterization of Cu<sub>60</sub>Zr<sub>40</sub> Nanoglasses

For the experiments, three amorphous Cu<sub>60</sub>Zr<sub>40</sub> films with different characteristics were produced using MS.<sup>[2]</sup> Two different

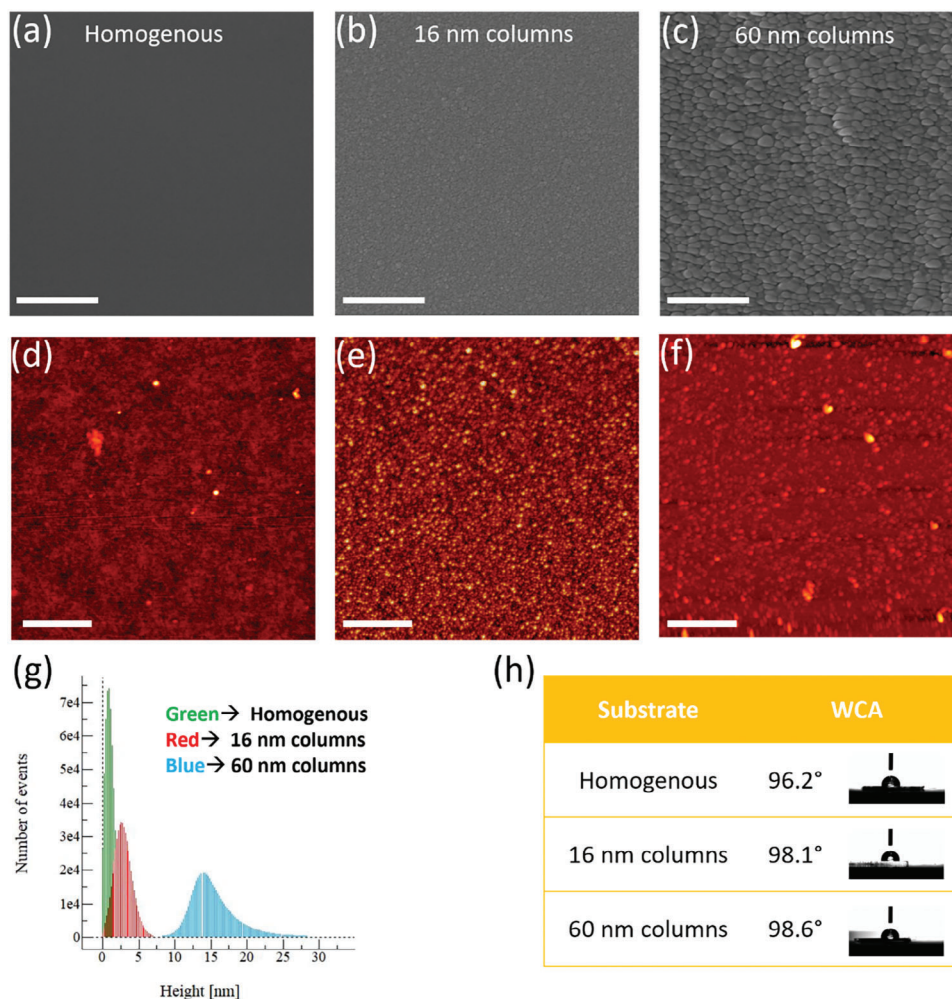


**Figure 2.** SEM images of surface topography of a) homogenous, b) 16 nm columns, and c) 60 nm columnar films. Scale bars for (a–c) equal 200 nm. Surface morphologies of the thin films d) homogenous, e) 16 nm columns, and f) 60 nm columns, and the corresponding roughness height distributions of (d–f) are shown in (g) respectively. The water contact angle of the surfaces is shown in (h), and three positions on each sample were probed. Scale bar for (d–f) equal 1  $\mu$ m.

sputtering systems were used for the growth of the amorphous films. The homogenous amorphous film and the nanoglass film with the 16 nm columns were prepared using RF magnetron sputtering, while DC magnetron sputtering was employed to grow the nanoglass film with the 60 nm columns. The variation of the column's size in the films was achieved by a variation of the pressure of the sputtering gas and by using different sputtering systems. The films were characterized using scanning electron microscopy (SEM) to determine the structure of the films and the size of the columns (Figure 2a–c). Additionally, as surface roughness plays an important role in lipid writing, the surface morphology of the films was characterized using AFM. Significant differences in average roughness were observed in the samples ((0.1  $\pm$  0.1), (0.8  $\pm$  0.1), and (2.8  $\pm$  0.6) nm for homogenous, 16 nm, and 60 nm substrates, respectively) as shown in Figure 2d–f. Water contact angle (WCA) was measured for all three substrates and is provided in the form of a table in Figure 2h.

## 2.2. Lipid Dip-Pen Nanolithography on Nanoglasses

The schematic of the L-DPN writing process and the lipid patterns written in this study are shown in Figure 1. A solution of 70 mol% DOPC and 30 mol% 1-palmitoyl-2-oleoyl-sn-glycero-3-phospho-L-serine (POPS) was used as a lipid mixture for L-DPN. In general, a plethora of different lipid mixtures are used as biomimetic models for the cell membrane.<sup>[33]</sup> Therefore, the choice of specifically a DOPC/POPS mixture is somewhat arbitrary but was made for its good performance in L-DPN, combined with its widespread use in biophysical studies. The mixture was doped with 1 mol% of 1,2-dioleoyl-sn-glycero-3-phosphoethanolamine-N-(Lissamine rhodamine B sulfonyle) (Rho-PE) to enable imaging of the written structures via fluorescence microscopy. As a test pattern for L-DPN (ensuring different writing directions and angles in regard to the writing tip) triangle-, square- and T-shapes with hatch lines of 400 nm distance were defined in the control software (Figure 1c).

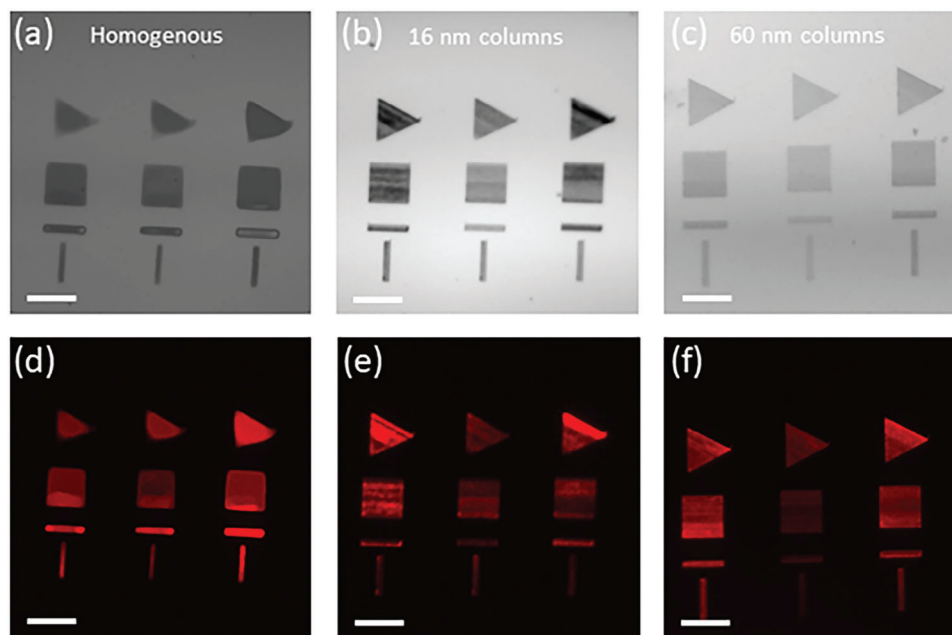


**Figure 3.** Optical bright field and corresponding fluorescence microscopy images of patterned phospholipid structures on a,d) homogenous  $\text{Cu}_{60}\text{Zr}_{40}$ , b,e) 16 nm columns, and c,f) 60 nm columns. The lipid structures on homogenous film show – in contrast to the ones on the columnar nanoglasses – spreading of the lipids resulting in less defined structures. Scale bars equal 15  $\mu\text{m}$  for all images.

The same conditions and pattern were used to print a neutral lipid mixture with DOPC and rhodamine onto these substrates (Figure S1, Supporting Information).

L-DPN could be implemented on all three films and resulted in the predesigned shapes (Figure 3). However, one striking difference is already visible in the optical micrographs: on the homogenous substrate, the hatch lines have clearly merged, as the patterns are smooth, while separate hatch lines can be still distinguished on the columnar nanoglasses. Also, the outline of the various shapes is less defined on the homogenous substrate. This difference indicates a higher spreading of the lipid membrane stacks on the surface of the homogenous substrate. Surface wettability is a main driver for the spreading of lipid features in L-DPN and thus the merging of the hatch lines. When a substrate is hydrophilic enough that L-DPN leads to a “heads to substrate” membrane configuration, as it is usually the case on glass and silicon oxide surfaces, in air, the written membranes will form single monolayers with stacks of “tail out” membranes on top.<sup>[34]</sup> On substrates of sufficient hydrophobicity, L-DPN will result in a “tails to substrate” membrane configuration, leading to direct stacks of “tail out” membranes in air, without an underlying monolayer.<sup>[24]</sup> These different orientations and stack types were also observed, e.g., in comparisons of L-DPN outcomes on graphene oxide (hydrophilic) and graphene (hydrophobic), as corroborated by molecular dynamics simulations.<sup>[35]</sup>

Also, the liquid spreading of lipids will result in mono-/bilayer depending on substrate hydrophobicity/-philicity.<sup>[36]</sup> L-DPN generated structures (in air) tend to spread more on more hydrophilic substrates (with lower WCA indicating a higher-energy surface) as, e.g., observed in comparisons of glass and polystyrene,<sup>[23]</sup> or self-assembled hydrophilic/hydrophobic monolayers,<sup>[32]</sup> as substrates for L-DPN. However, it should be noted that exceptions of

this general tendency were observed in “tails out” L-DPN written membranes on graphene, probably because of the strong interaction between graphene and the phospholipid carbon tails.<sup>[24]</sup> Overall, spreading behavior in L-DPN could be seen as analog to the spreading behavior of supported lipid bilayers in liquid,<sup>[37]</sup> though it should be noted that the mobility of lipids is generally higher in water than in an air environment, which can be used to merge L-DPN created hatch lines to full membranes on transfer into liquid.<sup>[38]</sup> However, in the present study, the WCA for all three surfaces is very similar ( $96.2 \pm 0.6^\circ$ ,  $98.1 \pm 3.3^\circ$ , and  $98.6 \pm 1.6^\circ$  for homogenous, 16, and 60 nm, respectively, see Figure S2, Supporting Information) and these differences in WCA seem not large enough to explain the huge difference in the spreading behavior. Also, the different roughness of the glasses, while significant, does not seem sufficient to explain the different spreading behavior. While nanoroughness can impact the phase state and thus mobility of lipids in liquid,<sup>[39]</sup> the roughness difference between homogeneous and 16 nm columnar nanoglass (0.1–0.8 nm) is of the same order of magnitude as in common L-DPN substrates showing no such abrupt change in spreading (e.g., silicon with native oxide layer  $\approx 0.1$  and glass surfaces  $\approx 0.2$ – $1.9$  nm).<sup>[40–42]</sup>

### 2.3. Characterization of Spreading and Deposition Volume

To get a better insight into the lipid structure morphology, AFM imaging was conducted on the samples. Differences in the surface structure were observed despite the fact that the writing conditions were kept constant for all substrates. The lipids form flat layers on the homogenous substrate with a height of  $\approx 6$  nm (Figure 4a). On the contrary, for the 16 nm (Figure 4b) and

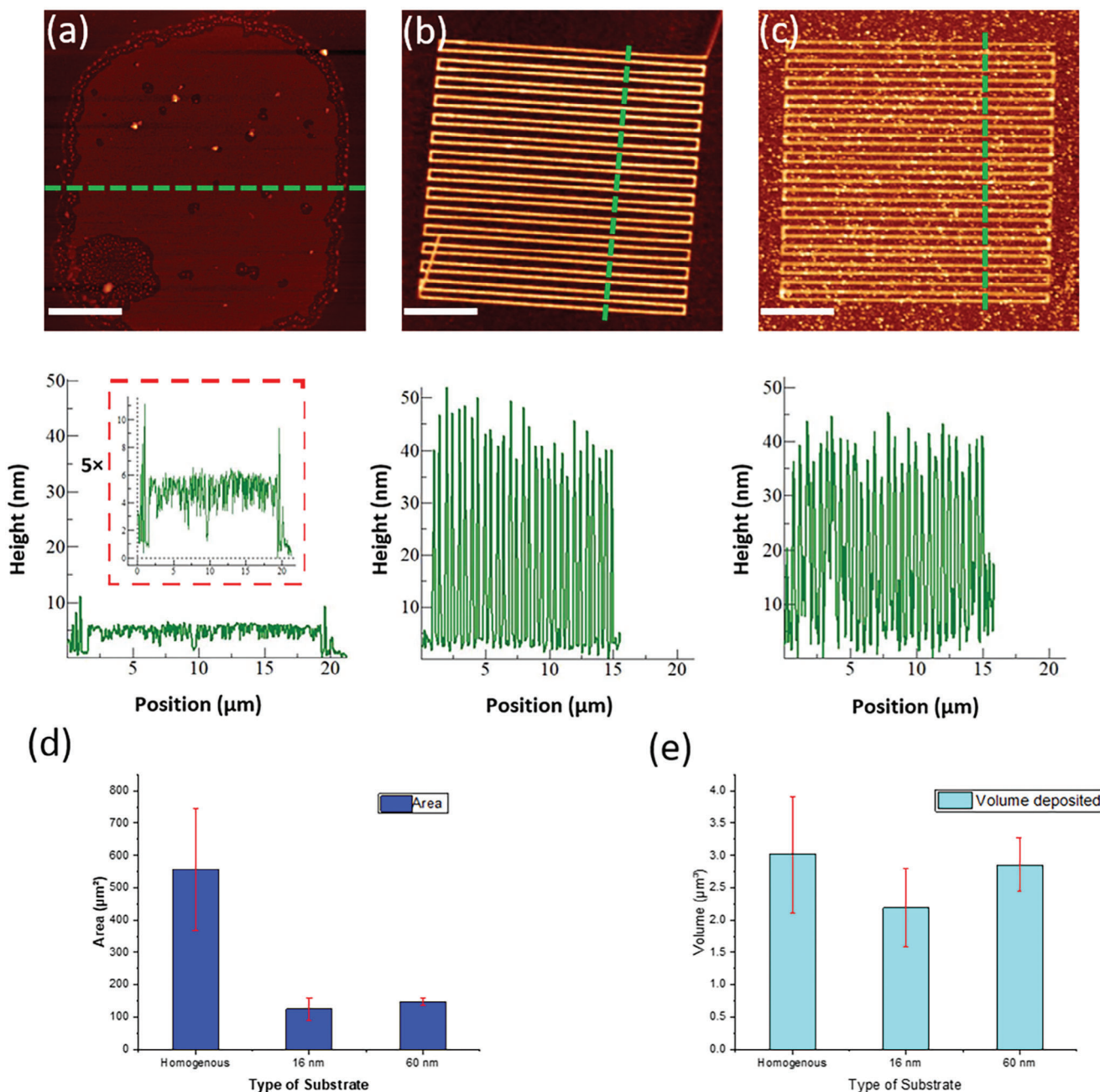


**Figure 4.** AFM topographic images after lipid patterning on different substrates. a) The homogenous film shows the complete spreading of lipids and the corresponding profile shows a height of 6 nm. b) 16 nm film shows stability of lipids with heights of 50 nm. c) 60 nm columnar also shows good stability with a variable height of 30 nm. Panels (d) and (e) show the average area and volume of the lipids patterned (from six measurements each). Scale bars are 4  $\mu\text{m}$ .

60 nm (Figure 4c) columnar substrates, the hatch lines (400 nm pitch) of the lipid structures are clearly visible and have mean heights of  $\approx 50$  and 30 nm, respectively. Systematic experiments with the same writing conditions and freshly prepared substrates were performed, and data on the average area covered and average volume deposited were calculated from AFM images to quantify the differences in spreading behavior. Figure 4e shows the average area of square structures for the different substrates and Figure 4f is a comparison of the average volume deposited

during printing. Also, additional surface characterization using SEM was performed for overview (Figure S3, Supporting Information).

Overall, the results show (as writing conditions are constant for all substrates) that the confinement of the phospholipids on the columnar nanoglasses leads to more defined lipid structures, while the material flow to the surface remains the same, hence the deposited volume stays nearly constant, while the covered area is reduced. Accordingly, the structures (as not being able to

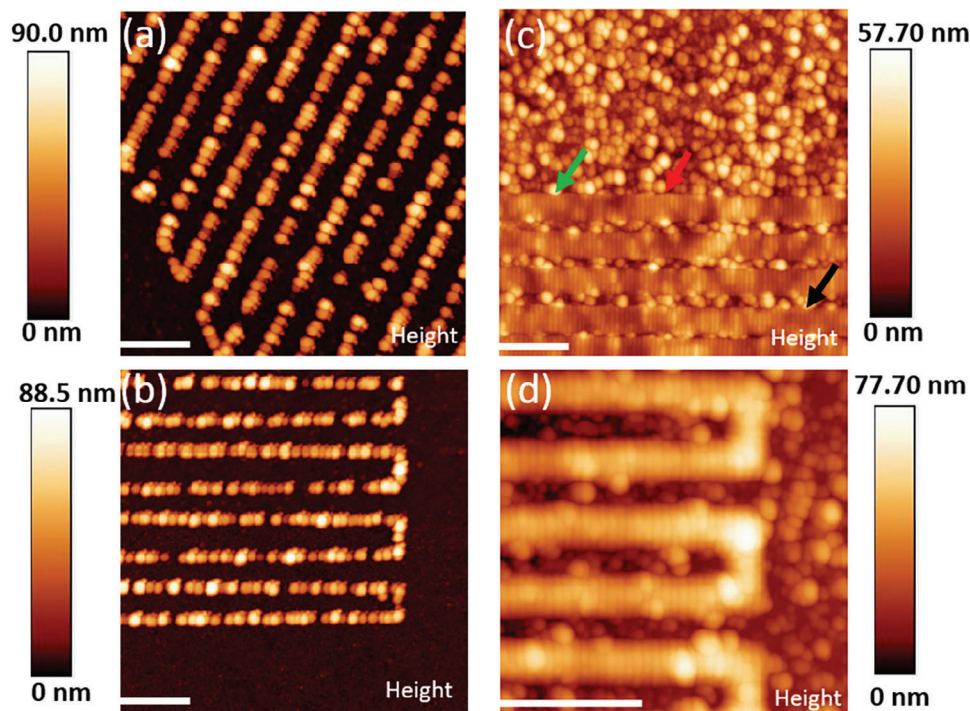


**Figure 5.** Zoomed-in AFM images of square and triangle patterns of lipids from the a,b) 16 nm and c,d) 60 nm columnar substrates. The arrows in (c) indicate the step pinning arrangement. The scale bar equals 1  $\mu\text{m}$  for all images.

spread out) are higher on the columnar nanoglasses compared to the flat, spread-out structures on the homogenous glass.

#### 2.4. Nanoscale Confinement of Phospholipids on Columnar Nanoglasses

Looking deeper into the details of the patterns on the columnar substrates through AFM, the most striking observations from the data (Figure 5) show that the lipids arrange themselves in peculiar structures of regular lines perpendicular to the hatch line writing direction.

On noncontinuous hatch lines (Figure 5a,b), peculiar grenade-shaped lipid patches are observed that align perpendicular to the writing direction. While the supporting nanoglass has an average column size of 16 nm, these objects have a diameter (along the writing line) of  $(110 \pm 33)$  nm for the main feature, and  $(42 \pm 9)$  nm for the smaller side feature. In order to eliminate the possibility of a double-tip imaging artifact, the structures were re-scanned using a new tip. It should also be mentioned that the columnar features of the substrate do not display any side features. The most probable explanation for this is that these features were unintentionally formed during the writing process, possibly due to the writing DPN tip picking up some material and creating a double tip. However, this accidental occurrence has allowed us to make an interesting observation: the nanoconfinement on the nanoglass enables the creation of even smaller features than those typically achievable in L-DPN, where the usual line width is  $\approx 100$  nm.

On the continuous hatch lines (Figure 5c,d), the regular pattern is condensed into stripes perpendicular to the hatch line

writing direction. While on the sample in Figure 5c,d a 60 nm column size substrate was used, the periodicity of the perpendicular stripes is  $(44 \pm 6)$  nm, thus even smaller than the object size on the 16 nm columnar substrate. These nanoscale arrangements were not found in all written patterns and seem to wane with increased structure height (Figure S4 and Table S1, Supporting Information) and form perpendicular to the fast-writing direction of the tip (Figure S5, Supporting Information). This implies a substrate-mediated influence either during writing or on reorganization after writing that can shape the immediate membrane layers, while additional layers are more and more decoupled. On the other hand, the object size and periodicity of stripes do not line up with the domain sizes of the substrate, showing that this phenomenon cannot be attributed purely due to alignment with underlying domains.

However, the close-up on hatch lines shows that the confinement and stability of the lipids into the hatch lines (in contrast to the spreading on the homogenous samples) seems to be linked to interfacial regions of the nanoglasses, although not to purely mechanical edge pinning, as stopping of the lipid spread is observed for boundaries between columns of different height (Figure 5c, high-to-low green arrow, low-to-high black arrow), but also for similar height columns (red arrow).

### 3. Conclusion

We have shown that phospholipid membranes can be patterned on different amorphous substrates of  $\text{Cu}_{60}\text{Zr}_{40}$  (homogenous and columnar) with sub-micron resolution using L-DPN (Figure 6a). These substrates show striking differences in the spreading of lipids with the columnar nanoglasses confining the

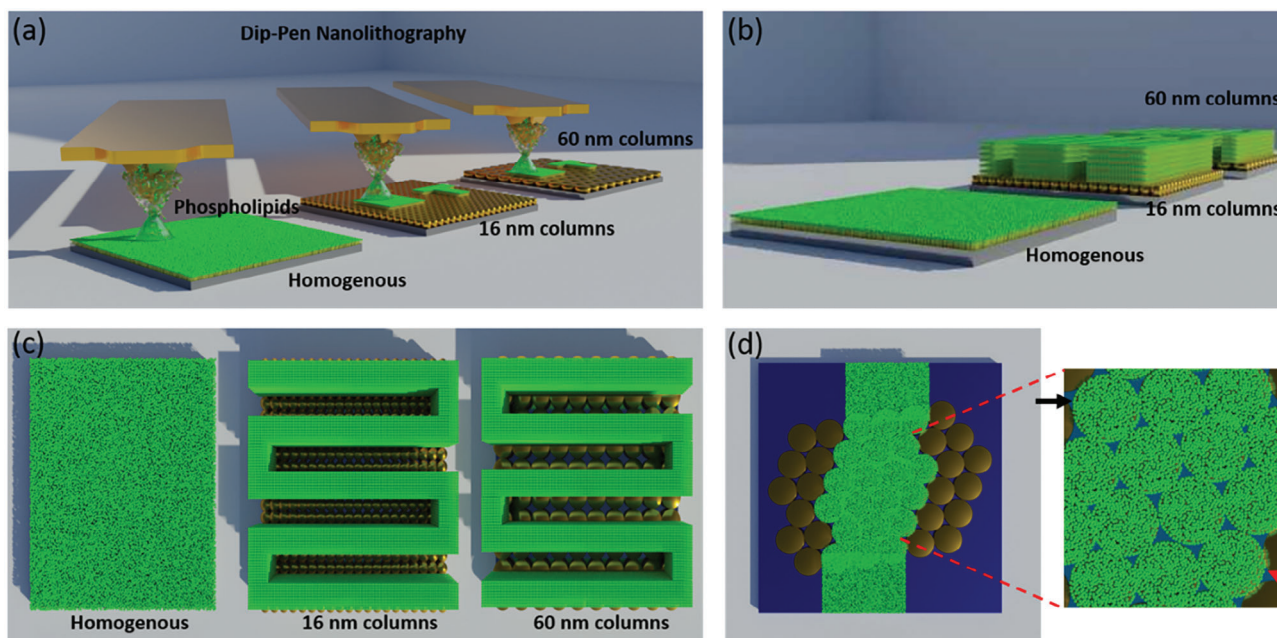


**Figure 6.** Schematic Illustration of the lipid organization on homogenous, 16 and 60 nm columnar nanoglasses. a) Patterning of phospholipids using L-DPN. b,c) Side and top views of lipid organization after patterning. d) Scheme of stabilization of the written phospholipid lines by stopping spreading at the boundaries of the columnar nanoglasses. The inset shows a magnified image of the influence of columnar boundaries (red and black arrows) on the stabilization of the phospholipids after writing.

lipids much stronger than the homogenous of the same composition (Figure 6b). Based on our results we propose the following picture of the nanoscopic lipid membrane organization on these substrates (Figure 6).

The confinement of lipid structures on columnar nanoglasses can be attributed to the influence of amorphous interfaces present in the 16 and 60 nm columnar substrates, which hinder spreading. Sub-structures observed for the lower layers of the lipid hatch-lines revealed a peculiar type of self-organization that could be connected to meniscus instabilities during the writing process (reminding to stripe pattern phenomena in Langmuir-Blodgett (LB) transfer of phospholipids<sup>[43]</sup>) and/or subsequent reorganization influenced by the nanoglass substrate. In this analogy, the oscillating water meniscus in the LB transfer, leading to liquid-expanded/liquid-condensed (LE/LC) phase monolayer deposition in alternating stripes is mimicked by the water meniscus building between the DPN tip and the nanoglass surface. While in LB transfer the substrate is lifted through the water meniscus, in DPN the meniscus itself is moved over the substrate by the DPN tip, resulting in a very similar relative motion and geometry in both cases. Similarly, the surface could induce or stabilize a ripple phase of ordered/unordered membrane parts in the written lipid lines, as can be observed as a separate lipid bilayer phase as an intermediate state during phase transition in lipid bilayers.<sup>[44–46]</sup> This could also lead to the fading observed with additional layers, as the layers get farer away and more decoupled from the surface.

The reported experiment (being done with model lipid membranes and in air rather as in liquid) is still different from a realistic biological cell/nanoglass interface. Yet, the discovery of distinct differences between homogenous amorphous substrates

and nanoglasses in regard to lipid-surface interaction that does not rely on the surface geometry, but rather on the presence of the columnar interfaces themselves, allows for the first time a plausible explanation for the distinct differences in cell behavior not present in chemically and topographically similar surfaces. As many processes in cells are modulated by the state and fine structure of their lipid membranes (e.g., through lipid-modulated proteins), nanoglass surfaces could give unique stimuli to cells by influencing their lipid membranes. Although research on the structure and properties of columns and interfaces in nanoglass thin films is scarce, knowledge is expanding for the CuZr system.<sup>[5]</sup> Hopefully, in the future a correlation between the experimental observations presented in this work and structural studies will be established, leading to a better understanding of the process governing lipid-nanoglass surface interactions. Then it would be possible to produce nanoglass films with the required properties by either alloying CuZr or using systems of other chemical composition. Furthermore, a detailed characterization of the interfacial area between the nanoglass columns could reveal the specific molecular mechanism behind the confinement effect. The results of the present study can motivate future studies with more realistic bio-membrane models or living cells that could look specifically for these kinds of interactions.

#### 4. Experimental Section

**Materials:** All phospholipids, i.e., DOPC (1,2-dioleoyl-sn-glycero-3-phosphocholine), POPS (1-palmitoyl-2-oleoyl-sn-glycero-3-phospho-L-serine (sodium salt) and Rho-PE (1,2-dioleoyl-sn-glycero-3-phosphoethanolamine-N-(Lissamine rhodamine B sulfonyl)) were

purchased from Avanti Polar Lipids (USA). The chloroform used as solvent was HPLC grade, from Sigma–Aldrich (Germany).

**Magnetron Sputtering:** Two different sputtering systems were used for the growth of the amorphous films. The homogenous amorphous film and the nanoglass film with the 16 nm columns were prepared using RF magnetron sputtering, while DC magnetron sputtering was employed to grow the nanoglass film with the 60 nm columns.

In the case of RF magnetron sputtering an alloy target of nominal composition of Cu<sub>60</sub>Zr<sub>40</sub> (at.%) was used. The sputtering system was used with a fixed distance between the substrate and target of 100 mm and a target tilt angle of 20°. A background pressure prior to deposition below  $5.0 \times 10^{-8}$  mbar was reached in the chamber. Thin films were deposited continuously on Si (100) wafers with a native oxide layer. Sputtering was performed with the temperature of a substrate of 293 K and power of 100 W with a substrate rotation velocity of 10 rpm. Films of two types: homogenous and columnar (16 nm columns) were prepared. Homogenous films were deposited at a working pressure of  $2.8 \times 10^{-3}$  mbar and a constant Ar flow rate of 40 sccm. Columnar films were deposited at a working pressure of  $8 \times 10^{-3}$  mbar and a constant Ar flow rate of 100 sccm.

In the case of DC magnetron sputtering, the thin film samples were prepared by co-sputtering using two elemental targets of Cu and Zr with varying applied power. The sputtering system was used with a fixed distance between the substrate and target of 100 mm and a target tilt angle of 38°. The background pressure before deposition below  $5.0 \times 10^{-8}$  mbar was reached in the chamber. Thin films were deposited continuously on Si (100) wafers with a native oxide layer. Sputtering was performed with the temperature of the substrate of 293 K without the rotation of the substrate. Columnar films (60 nm columns) were produced using voltages of 80 V for Cu target, 100 V for Zr target, and a working pressure of  $8 \times 10^{-3}$  mbar.

The sputtering time was adjusted to produce films with a thickness of  $\approx 200$  nm. The thickness of the films was measured with a Veeco Dektak 6 M Stylus Profiler.

**Lipid Dip-Pen Nanolithography (L-DPN):** The microfluidic inkwell (ACST, U.S.A.) was filled with 1  $\mu$ L of lipid mixture (70 mol% DOPC and 30 mol% POPS). Lipid patterns were written using the DPN5000 system (Nanoink, U.S.A) with F-type cantilevers (ACST, U.S.A.) containing individual 32 pens. The cantilevers were mounted onto a holder and then dipped with the lipid mixture using a microfluidic inkwell at high humidity ( $\approx 75\%$ ). A series of test patterns were written on a clean Si substrate to remove excess lipid ink before moving to the nanoglass substrates. Here, for all experiments writing parameters were kept the same at  $2 \mu\text{m}^{-1}$  sec writing speed and 40% R.H.

**Atomic Force Microscopy (AFM):** To inspect the surface topography, AFM imaging was done in ambient conditions with Dimension Icon from Bruker in tapping mode. Tap300AI-G (Budget Sensors) probes were used for the imaging with resonance frequency of 300 kHz and force constant of  $40\text{N m}^{-1}$ . Images were analyzed using WSxM software.<sup>[47]</sup> Written area/deposited volume was determined by the flooding tool from two square features on three different samples (so six measurements) for each substrate type.

**Water Contact Angle (WCA):** The surfaces of the substrates were characterized for contact angle using the OCA-20 system (DataPhysics Instruments GmbH, Filderstadt, Germany), by the sessile drop method. A dosing volume of 3.0  $\mu$ L was used and three measurements were performed on each sample.

**Optical Microscopy:** Microscopy images of the lipid patterns were acquired using a Nikon Eclipse 80i upright fluorescence microscope (Nikon, Germany) equipped with an Intensilight illumination (Nikon, Japan), a DSQi2 camera (Nikon, Germany) using a TexasRed filter.

**Scanning Electron Microscopy (SEM):** SEM LEO-1530 was used to study the morphology and stability of films on various substrates. The acceleration voltage and the working distance were 20 kV and 3.1 mm, respectively.

**Statistical Analysis:** Generally, the results of the experiments were reported as mean  $\pm$  standard deviation. For the reported WCA, three different random positions were probed on each of the three different sample types. Data for the height distribution histogram and roughness values were obtained from WSxM with the roughness analysis tool from the pre-

sented images. The size of the grenade-shaped lipid features was determined manually from randomly selected features ( $n = 20$  for the bigger,  $n = 34$  for the smaller side features) with WSxM. The stripe feature size was measured with WSxM along the respective lipid feature line in the image from 28 features. Means and SD were calculated in Excel and plotted in Origin.

## Supporting Information

Supporting Information is available from the Wiley Online Library or from the author.

## Acknowledgements

S.K.V. acknowledges Lahari Yaddanapudi and George Mathew for their help with the schematics. This work was carried out with the support of the Karlsruhe Nano Micro Facility (KNMF), a Helmholtz Research Infrastructure at Karlsruhe Institute of Technology (KIT). H.H. and E.B. acknowledge the financial support of the Deutsche Forschungsgemeinschaft under contract HA 1344/46-1.

Open access funding enabled and organized by Projekt DEAL.

## Conflict of Interest

The authors declare no conflict of interest.

## Data Availability Statement

The data that support the findings of this study are available from the corresponding author upon reasonable request.

## Keywords

lipid membranes, nanoglasses, scanning probe lithography, spreading behavior

Received: August 29, 2023

Revised: October 20, 2023

Published online:

- [1] H. Gleiter, *Beilstein J. Nanotechnol.* **2013**, *4*, 517.
- [2] S. H. Nandam, Y. Ivanisenko, R. Schwaiger, Z. Sniadecki, X. Mu, D. Wang, R. Chellali, T. Boll, A. Kilmametov, T. Bergfeldt, H. Gleiter, H. Hahn, *Acta Mater.* **2017**, *136*, 181.
- [3] S. H. Nandam, O. Adjaoud, R. Schwaiger, Y. Ivanisenko, M. R. Chellali, D. Wang, K. Albe, H. Hahn, *Acta Mater.* **2020**, *193*, 252.
- [4] N. Chen, R. Frank, N. Asao, D. V. Louzguine-Luzgin, P. Sharma, J. Q. Wang, G. Q. Xie, Y. Ishikawa, N. Hatakeyama, Y. C. Lin, M. Esashi, Y. Yamamoto, A. Inoue, *Acta Mater.* **2011**, *59*, 6433.
- [5] H. Voigt, A. Rigoni, E. Boltynjuk, M. R. Chellali, B. Tyler, H. Rösner, S. Divinski, H. Hahn, G. Wilde, *Adv. Funct. Mater.* **2023**, *33*, 2302386.
- [6] Y. Ivanisenko, C. Kübel, S. H. Nandam, C. Wang, X. Mu, O. Adjaoud, K. Albe, H. Hahn, *Adv. Eng. Mater.* **2018**, *20*, 1800404.
- [7] R. S. Averbach, H. Hahn, H. J. Höfler, J. C. Logas, *Appl. Phys. Lett.* **1990**, *57*, 1745.
- [8] P. Gong, X. Wang, Y. Shao, N. Chen, X. Liu, K. F. Yao, *Intermetallics* **2013**, *43*, 177.



- [9] S. V. Ketov, X. Shi, G. Xie, R. Kumashiro, A. Y. Churyumov, A. I. Bazlov, N. Chen, Y. Ishikawa, N. Asao, H. Wu, D. V. Louzguine-Luzgin, *Sci. Rep.* **2015**, *5*, 7799.
- [10] N. Chen, X. Shi, R. Witte, K. S. Nakayama, K. Ohmura, H. Wu, A. Takeuchi, H. Hahn, M. Esashi, H. Gleiter, A. Inoue, D. V. Louzguine, *J. Mater. Chem. B* **2013**, *1*, 2568.
- [11] I. Casanellas, J. Samitier, A. Lagunas, *Front. Bioeng. Biotechnol.* **2022**, *10*, 1002967.
- [12] K. Modaresifar, S. Azizian, M. Ganjian, L. E. Fratila-Apachitei, A. A. Zadpoor, *Acta Biomater.* **2019**, *83*, 29.
- [13] S. Namgung, T. Kim, K. Y. Baik, M. Lee, J.-M. Nam, S. Hong, *Small* **2011**, *7*, 56.
- [14] L. Richert, F. Vetrone, J.-H. Yi, S. F. Zalzal, J. D. Wuest, F. Rosei, A. Nanci, *Adv. Mater.* **2008**, *20*, 1488.
- [15] X. Shi, S. Chen, J. Zhou, H. Yu, L. Li, H. Wu, *Adv. Funct. Mater.* **2012**, *22*, 3799.
- [16] L. Xiao, Y. Sun, L. Liao, X. Su, *J. Mater. Chem. B* **2023**, *11*, 2550.
- [17] J. Luo, M. Walker, Y. Xiao, H. Donnelly, M. J. Dalby, M. Salmeron-Sanchez, *Bioact Mater* **2022**, *15*, 145.
- [18] S. Cao, Q. Yuan, **2022**.
- [19] D. Marsh, *Biochim. Biophys. Acta* **2008**, *1778*, 1545.
- [20] T. W. Lowry, A. E. Kusi-Appiah, D. A. Fadool, S. Lenhart, *Membranes* **2023**, *13*, 151.
- [21] R. D. Piner, J. Zhu, F. Xu, S. Hong, C. A. Mirkin, *Science* **1999**, *283*, 661.
- [22] G. Liu, M. Hirtz, H. Fuchs, Z. Zheng, *Small* **2019**, *15*, 1900564.
- [23] S. Lenhart, P. Sun, Y. Wang, H. Fuchs, C. A. Mirkin, *Small* **2007**, *3*, 71.
- [24] M. Hirtz, A. Oikonomou, T. Georgiou, H. Fuchs, A. Vijayaraghavan, *Nat. Commun.* **2013**, *4*, 2591.
- [25] E. Berganza, E. Boltynjuk, G. Mathew, F. F. Vallejo, R. Gröger, T. Scherer, S. Sekula-Neuner, M. Hirtz, *Small* **2023**, *19*, 2205590.
- [26] A. E. Kusi-Appiah, N. Vafai, P. J. Cranfill, M. W. Davidson, S. Lenhart, *Biomaterials* **2012**, *33*, 4187.
- [27] S. Sekula, J. Fuchs, S. Weg-Remers, P. Nagel, S. Schuppler, J. Fragala, N. Theilacker, M. Franzreb, C. Wingren, P. Ellmark, C. A. K. Borrebaeck, C. A. Mirkin, H. Fuchs, S. Lenhart, *Small* **2008**, *4*, 1785.
- [28] H.-Y. Liu, R. Kumar, C. Zhong, S. Gorji, L. Paniushkina, R. Masood, U. A. Wittel, H. Fuchs, I. Nazarenko, M. Hirtz, *Adv. Mater.* **2021**, *33*, 2008493.
- [29] E. Berganza, M. P. Ebrahimkutty, S. K. Vasantham, C. Zhong, A. Wunsch, A. Navarrete, M. Galic, M. Hirtz, *Nanoscale* **2021**, *13*, 12642.
- [30] M. Hirtz, A. Oikonomou, N. Clark, Y.-J. Kim, H. Fuchs, A. Vijayaraghavan, *Nanoscale* **2016**, *8*, 15147.
- [31] H.-Y. Liu, R. Kumar, M. Takai, M. Hirtz, *Molecules* **2020**, *25*, 2768.
- [32] M. Gavutis, V. Navikas, T. Rakickas, S. Vaitekoniš, R. Valiokas, *J. Micromech. Microengineer.* **2016**, *26*, 025016.
- [33] A. Luchini, G. Vitiello, *Biomimetics* **2020**, *6*, 3.
- [34] M. Hirtz, R. Corso, S. Sekula-Neuner, H. Fuchs, *Langmuir* **2011**, *27*, 11605.
- [35] N. Willems, A. Urtizberea, A. F. Verre, M. Iliut, M. Lelimosin, M. Hirtz, A. Vijayaraghavan, M. S. P. Sansom, *ACS Nano* **2017**, *11*, 1613.
- [36] B. Sanii, A. N. Parikh, *Soft Matter* **2007**, *3*, 974.
- [37] I. Gözen, P. Dommersnes, A. Jesorka, I. Gözen, P. Dommersnes, A. Jesorka, in *Surface Energy*, IntechOpen, London, UK **2015**.
- [38] S. Sekula, J. Fuchs, S. Weg-Remers, P. Nagel, S. Schuppler, J. Fragala, N. Theilacker, M. Franzreb, C. Wingren, P. Ellmark, C. A. K. Borrebaeck, C. A. Mirkin, H. Fuchs, S. Lenhart, *Small* **2008**, *4*, 1785.
- [39] F. Blachon, F. Harb, B. Munteanu, A. Piednoir, R. Fulcrand, T. Charitat, G. Fragneto, O. Pierre-Louis, B. Tinland, J.-P. Rieu, *Langmuir* **2017**, *33*, 2444.
- [40] K. Mori, S. Samata, N. Mitsugi, A. Teramoto, R. Kuroda, T. Suwa, K. Hashimoto, S. Sugawa, *Jpn. J. Appl. Phys.* **2020**, *59*, SMMB06.
- [41] S. M. M. Dadfar, S. Sekula-Neuner, V. Trouillet, M. Hirtz, *Adv. Mater. Interfaces* **2021**, *8*, 2002117.
- [42] N. Chada, K. P. Sigdel, R. R. S. Gari, T. R. Matin, L. L. Randall, G. M. King, *Sci. Rep.* **2015**, *5*, 12550.
- [43] X. Chen, S. Lenhart, M. Hirtz, N. Lu, H. Fuchs, L. Chi, *Acc. Chem. Res.* **2007**, *40*, 393.
- [44] M. Majewska, D. Mrdenovic, I. S. Pieta, R. Nowakowski, P. Pieta, *Biochim. Biophys. Acta* **2020**, *1862*, 183347.
- [45] H. Takahashi, A. Miyagi, L. Redondo-Morata, S. Scheuring, *Small* **2016**, *12*, 6106.
- [46] C. Leidy, T. Kaasgaard, J. H. Crowe, O. G. Mouritsen, K. Jørgensen, *Biophys. J.* **2002**, *83*, 2625.
- [47] I. Horcas, R. Fernández, J. M. Gómez-Rodríguez, J. Colchero, J. Gómez-Herrero, A. M. Baro, *Rev. Sci. Instrum.* **2007**, *78*, 013705.